Effects of Impurities on Alumina-Niobium Interfacial Microstructures

Joseph T. McKeown, Joshua D. Sugar,
Ronald Gronsky, and Andreas M. Glaeser*

Department of Materials Science and Engineering,
University of California
&
Ceramic Science Program
Materials Sciences Division
Lawrence Berkeley National Laboratory,
Berkeley, CA 94720

Abstract

Optical microscopy, scanning electron microscopy, and transmission electron microscopy were employed to examine the interfacial microstructural effects of impurities in alumina substrates used to fabricate alumina-niobium interfaces *via* liquid-film-assisted joining. Three types of alumina were used: undoped high-purity single-crystal sapphire; a high-purity, high-strength polycrystalline alumina; and a lower-purity, lower-strength polycrystalline alumina. Interfaces formed between niobium and both the sapphire and high-purity polycrystalline alumina were free of detectable levels of impurities. In the lower-purity alumina, niobium silicides were observed at the alumina-niobium interface and on alumina grain boundaries near the interface. These silicides formed in small-grained regions of the alumina and were found to grow from the interface into the alumina along grain boundaries. Smaller silicide precipitates found on grain boundaries are believed to form upon cooling from the bonding temperature.

Keywords: alumina, niobium, ceramic-metal interfaces, purity, silicides

* Corresponding author. Tel.: 01-510-486-7262; fax: 01-510-486-6904.
E-mail address: aglaeser@sapphire.berkeley.edu.

Introduction

During the fabrication of ceramic-metal interfaces, impurities present in both the ceramic and metal can segregate to the interface and affect the fracture strength of the final assembly directly through their effect on interfacial adhesion and fracture path, and indirectly through their effect on plastic dissipation accompanying fracture [1-6]. Whether the effects of impurities are beneficial or detrimental depends on multiple factors, including the chemical species present and the formation of secondary phases.

The interfacial fracture energy, $\overline{G}_C$, of a ceramic-metal interface [1, 7, 8] is a function of the work of adhesion, W_{ad}, and the dissipated work of plastic deformation in the metal, W_p:

$$\overline{G}_C = W_{ad} + W_p \tag{1}$$

The plastic work has been shown to be a nonlinear function of the work of adhesion [7]:

$$W_p = \left(W_{ad}\right)^n \tag{2}$$

where n is an empirical parameter that is greater than unity and depends on the materials system.

Fracture in alumina-niobium assemblies generally occurs at the interface in diffusion-bonded samples processed with a dense, high-purity alumina. More generally, the fracture path and fracture energy are dependent on parameters such as alumina porosity, alumina purity, and impurity content of the niobium, which determine the interfacial microstructure and chemistry [1-6]. It is therefore of fundamental interest to understand the effects of impurities on the interfacial microstructure of an alumina-niobium interface.

Silicate phases can influence both the bonding process, and the fracture strength of bonded ceramic-metal interfaces. In studies of alumina-platinum interfaces [3], intervening amorphous and crystalline silicate phases were obtained by deposition of a silica layer onto the sapphire or alumina prior to bonding. Results showed that the amorphous phase played a dual role, accelerating the rate of diffusion bonding, leading to an interface with a small area fraction of defects and voids, but also

degrading the interfacial fracture energy. The fracture energy was not adversely affected by the presence of crystalline silicates.

Alumina-niobium is a widely studied ceramic-metal system with bonded interfaces that are virtually free of thermal stresses due to closely matched thermal expansion coefficients. Niobium and alumina are also chemically compatible, producing interfaces with no chemical reaction layer when bonded in vacuum [2, 9, 10]. Considerable prior research has been conducted on the mechanical properties and interfacial characterization of the alumina-niobium system [2, 9-17]. In the case of alumina-niobium interfaces, niobium silicide formation has been observed in previous studies [1, 4, 18]. In the present study, polycrystalline alumina substrates of two distinct purities and single-crystal alumina (sapphire) substrates were used to fabricate alumina-niobium interfaces by liquid-film-assisted joining (LFAJ). The presence of brittle phases at the interface due to interaction with intergranular glassy phases in the alumina was investigated using optical microscopy, scanning electron microscopy, and transmission electron microscopy.

Experimental Procedures

Interfaces were fabricated with three types of aluminum oxide: undoped, high-purity, single-crystal sapphire (typically ≈99.996% pure, Insaco Inc., Quakertown, PA); a high-purity, high-strength, fine-grain-size polycrystalline alumina (≈99.9% pure, SSA-999W, Nikkato Corp., Osaka, Japan); and a lower-purity, lower-strength, coarser-grain-size polycrystalline alumina (≈99.5% pure, AD995, Coors Technical Ceramic Co., Oak Ridge, TN). All assemblies were joined using a multilayer copper/niobium/copper interlayer with two ≈3.0-μm-thick copper layers flanking a 125-μm-thick 99.99% pure niobium foil (Goodfellow Corp., Malvern, PA). Assemblies were processed at 1400°C for 6 h with an applied load of ≈2 MPa in a graphite-element hot press. Samples were heated to the bonding temperature at 4°C/min and then cooled to room temperature at 2°C/min. During the bonding cycle, the copper melted to form a copper-rich liquid film that facilitated contact growth and bonding between the alumina and niobium. Details of the interface processing are available in prior publications [9, 17, 19, 20].

Assemblies were machined into beams approximately 4 cm long with a 3 mm × 3 mm cross-section. The interlayer was at the center of the length of the beams. The room-temperature fracture strength was determined using four-point bending.

Images of interfaces were taken in an optical microscope. Beams chosen for imaging were ultrasonically cleaned in isopropyl alcohol for approximately 15 min. Cross-sections of interfaces were prepared with a diamond saw and then ground flat on 30-μm diamond paper and polished with progressively finer diamond grit, ending with a 0.05-μm colloidal-silica suspension. Cross-sections were then cleaned in acetone and isopropyl alcohol for approximately 15 min each.

SEM samples were prepared in the same manner as cross-sections used for optical microscopy. Electron microscopy was performed in a Hitachi S-4300 SE/N FE SEM.

TEM specimens were prepared from beams that failed within the ceramic and along the interface. Cross-sectional samples of the interface were machined into 3-mm discs and thinned mechanically by grinding, polishing, and dimpling until the center of the disc was <20 μm thick. The dimple was polished to a 0.05-μm finish. Finally, a perforation was made in the center of the disc at the alumina-niobium interface by low-energy Ar^+ ions in an ion mill. Electron microscopy and energy dispersive spectrometry were performed in a JEOL 200CX and a Philips CM 200, both operating at an accelerating voltage of 200 kV.

Results and Discussion

Mechanical Properties of Assemblies

An assembly processed with sapphire substrates used undoped sapphire with the *c*-plane (0001) as the joining surface. All beams from this assembly failed along the sapphire-niobium interface at tensile stresses ≤177 MPa [19]. Breakup of the initially continuous copper film during bonding was incomplete, leaving large patches of relatively weak copper-alumina interface along the bond plane that may account for the low strengths and the propensity for interfacial failure.

In joints prepared with polycrystalline alumina, disruption of the initially continuous copper film is more extensive, and the area fraction of alumina-niobium contact is higher. Joint

properties were sensitive to the alumina characteristics. Joints processed using 99.9%-pure alumina had a higher average fracture strength (359 MPa) than those prepared with 99.5%-pure alumina (241 MPa) [19]. All of the 99.9%-pure alumina joints and ≈75% of 99.5%-pure alumina joints failed entirely in the alumina, and thus the relative fracture strengths reflect the differences in the alumina fracture properties. Grain size is the major factor responsible for this higher fracture strength. The average grain size is larger than or on the order of the size of flaws created during processing, so the defect that determines the strength scales with the average grain size. The average strength of beams prepared from the unbonded as-received 99.9%-pure alumina was ≈560 MPa [19]. Comparing grain sizes in as-received and bonded 99.9%-pure alumina, the mean linear intercepts were ≈0.9 and ≈1.2 μm, respectively [19]. The 99.5%-pure alumina exhibited a bimodal grain size distribution, with the larger mode being ≈25 μm. A roughly linear relationship between strength and the inverse square root of grain size was previously reported in studies examining the grain size dependence of the fracture strength of a similar high-purity alumina [21]. A smaller grain size increases the number of initial contacts at the alumina-niobium interface during the bonding cycle, thus leading to increased void elimination at the interface.

The shift to ceramic failures in bonds prepared with polycrystalline aluminas indicates that the strength of the alumina-interlayer interface generally exceeded that of the adjoining alumina. Since all bonds involving 99.9%-pure alumina failed in the ceramic, fracture surfaces alone provide no insight on the alumina-interlayer interfacial microstructure and chemistry. In joints processed with 99.5%-pure alumina, examination of interfacial fracture surfaces was possible and revealed the presence of adherent islands of a silicide phase and tearing of niobium in bonded regions where the niobium was in contact with the finer-grain-size alumina regions [18, 20, 24]. This indicated that the small amount of glassy silicate phase present in the material may play a role in alumina-niobium contact formation and does modify the alumina-niobium interfacial microstructure.

Interface Characterization

Single-Crystal Sapphire Substrates

Figure 1 is an optical micrograph of a sapphire-niobium interface in cross-section. The interface appears distinct and smooth. There are also no reaction phases present at the interface, as expected [1, 16, 19, 22]. Sapphire eliminates the possibility of a glassy phase flowing to and filling interfacial voids [19]. Copper particles persist at the interface after bonding due to the low solubility of copper in niobium and a low rate of copper-niobium interdiffusion. These ductile particles affect the fracture strength of the joined assembly in a manner that depends specifically on the morphology and volume fraction of the copper [18, 20, 23, 24]. The inset in Figure 1 shows two of these copper particles at increased magnification. There are two distinct copper particle morphologies, labeled "a" and "b." The particle labeled "a" is copper trapped in a niobium grain-boundary groove. The grain boundary is not evident in the micrograph, but SEM images and chemical etching clearly show the boundary. The particle labeled "b" forms as a result of copper film dewetting. Figure 2 is an SEM image of a sapphire-niobium interface in cross-section. The interface is free of secondary phases. Deviations from planarity are a result of local roughness on the surface of the sapphire. Energy-dispersive spectrometry (EDS) in both the SEM and TEM confirms that the interface is free of detectable levels of impurities.

High-Purity (99.9%-Pure) Polycrystalline Alumina Substrates

Figure 3 is an optical micrograph of the alumina-niobium interface. Figure 4 is an SEM image of the same interface at higher magnification. The interface is free of secondary phases, consistent with expectations of a high-purity alumina, and appears rough on the scale of the alumina grain size due to the grooving of the alumina grains during bonding. The niobium has conformed to the alumina surface, penetrating into the alumina grain-boundary grooves. Again, EDS in both the SEM and TEM detected no impurities.

Lower-Purity (99.5%-Pure) Polycrystalline Alumina Substrates

Figure 5 shows a cross-sectional optical micrograph of an alumina-niobium interface processed using 99.5%-pure alumina. Small silicide precipitates are evident at and slightly away

from the interface. The interface again appears rough due to grain-boundary grooving, and fractography shows that the silicide precipitates are present in small-grained regions of the alumina. This is due to a higher grain-boundary density in these regions, leading to a higher silicon flux per unit area of alumina and a higher local concentration of silicon at the interface during bonding as a result of the glassy phase flowing to wet the interface. The boxed regions labeled "a" and "b" correspond to the SEM images of silicide precipitates at and near the alumina-niobium interface in, respectively, Figures 6 and 7. The precipitates that are situated away from the interface lie along alumina grain boundaries.

In Figure 6, the precipitates labeled ① lie ≈1.5 μm away from the larger precipitates. The precipitate labeled ② is ≈1 μm away from the alumina-niobium interface. Figure 8 is a bright-field TEM image of a silicide precipitate at the alumina-niobium interface. In Figure 6, 7, and 8, the silicide precipitates extend ≈4 μm along alumina grain boundaries. Figure 9 shows what appears to be a small isolated precipitate situated ≈0.2 μm away from the interface. It should be noted that these distances are in the plane of observation. If a precipitate is inclined relative to the interface, the observed and actual morphology and microstructure may be slightly different due to sectioning during sample preparation.

EDS in the SEM indicates that the precipitates contain both niobium and silicon. A sample spectrum from the precipitate in Figure 7 is shown in Figure 10. EDS with a 10-nm probe size was conducted in the TEM. Figure 11 shows EDS spectra obtained from two locations within the silicide in Figure 8, from a grain at the alumina-niobium interface and from an adjacent grain farther from the interface. The scales in Figures 10 and 11 reflect the intensity of each peak relative to the intensity of the Nb L peak. The iron and chromium peaks in the spectra are a result of ion milling residuals. The copper peak is due to incorporated copper, present as a result of the liquid-film-assisted joining technique. The silicide composition was found to vary with microstructural location (*i.e.*, proximity to the alumina-niobium interface). The energy scales for the two spectra in the figure are offset by 2 keV to facilitate a side-by-side comparison of the niobium and silicon peak heights, and to show the change in the Nb:Si peak height ratio. In the binary niobium-silicon phase

diagram [25], Nb_5Si_3 coexists with niobium at 1400°C, and is stable over a narrow range of composition. The ternary niobium-silicon-copper system has only been studied at 800°C and 875°C [26]; there is little copper incorporation in the silicides, and little adjustment in the stoichiometry ranges for silicide stability. In the present study, EDS indicates the Nb:Si ratio of the silicide at the interface is ≈4.5:3, and that the phase incorporates ≈5.5 atomic % copper. The Nb:Si ratio agrees with the EDS results of Kruzic *et al.* [18] from adherent islands of silicide precipitates on alumina fracture surfaces. The composition *vis-a-vis* the binary phase diagram and available isothermal ternary sections would suggest a mixture of ≈95% Nb_5Si_3 and ≈5% $NbSi_2$, however, the grain is single phase and electron diffraction analysis [27] indicates the structure is consistent with "Nb_5Si_3". In the adjacent grain, the spectrum was obtained from a region ≈1.5 μm from the interface. The Nb:Si ratio is 3.8:3, and the overall composition would again lie in the Nb_5Si_3 and $NbSi_2$ two-phase field [25], and contain ≈80% Nb_5Si_3 and ≈20% $NbSi_2$. However, the grain itself is again single phase. It seems unlikely that the signal was acquired from more than one grain through the thickness of the sample, or that there is a contribution from an adjoining grain. Instead, "Nb_5Si_3" may exist over a wider compositional range at 1400°C, and compositional variations with depth may be associated with diffusional growth of the phase. Further analysis of the phase (EDS, diffraction), microstructure (defect structure, orientation relationship), and mechanism of formation of these niobium silicide precipitates will be the subject of future research and publication.

The presence of niobium silicide precipitates both at and slightly away from the interface indicates two possibly distinct mechanisms for their formation. A glassy silicate phase is present at grain boundaries in the bulk alumina. At elevated temperatures, SiO_2 flows to the interface. In the case of precipitates at the interface, nucleation most likely occurs at the interface of the niobium metal in contact with alumina grain boundaries, and silicon that has diffused to the interface. The precipitate then grows into the alumina, down the grain boundary where the silicon concentration is higher. The presence of grain boundaries (see Figure 8) *within* the niobium silicide precipitates suggests more than one nucleation site along the grain boundary. These precipitates then grow and

impinge upon each other. The development of isolated precipitates on alumina grain boundaries at some depth below the alumina-niobium interface would seemingly require niobium diffusion down the alumina grain boundaries and locally favorable nucleation conditions. The small size of these particles suggests that nucleation and growth occurs during cooling. At temperature, the concentration of niobium should decrease with depth below the interface, and there should be an opposing gradient in the silica content. As the material is cooled, dissolved niobium will flow back to the niobium interlayer, resulting in a local niobium concentration maximum at some depth below the surface. As the temperature decreases, conditions suitable for silicide nucleation may develop at points where the supersaturation is highest.

Niobium silicides affect the interfacial adhesion, and therefore the interfacial fracture energy. Fractography and EDS data obtained from fracture surfaces [18, 20] indicate that the fracture path proceeded either along the Nb-Nb_5Si_3 interface or through the Nb_5Si_3 particle. The interfacial fracture energies of Nb-Nb_5Si_3 interfaces and Al_2O_3-Nb_5Si_3 interfaces have been reported as, respectively, ≥ 33.7 J/m^2 and ≈ 16 J/m^2 [28]. Nb_5Si_3 is a brittle phase, with $K_{IC} \approx 3$ MPa·m$^{1/2}$ [29]. It is possible that the crack initially propagated along the Al_2O_3-Nb_5Si_3 interface and then deviated either along the Nb-Nb_5Si_3 interface or through the silicide particle.

Conclusions

Examination of alumina-niobium interfaces processed *via* liquid-film-assisted joining using optical microscopy, SEM, and TEM revealed that niobium silicides form in samples fabricated with a low-purity polycrystalline alumina. Interfaces processed with single-crystal sapphire and high-purity polycrystalline alumina were free of detectable levels of impurities.

Silicide precipitates form at the alumina-niobium interface and along alumina grain boundaries near the interface. Silicides at the interface grow into the alumina grain boundaries. Smaller silicide precipitates along grain boundaries are believed to form upon cooling from the bonding temperature. The composition of silicide precipitates was found to depend on proximity

to the alumina-niobium interface. Precipitates at the interface and in physical contact with niobium were identified as Nb_5Si_3. At locations situated away from the interface, the niobium concentration was reduced. This suggests that copper incorporation widens the compositional stability range for "Nb_5Si_3" at elevated temperatures.

Acknowledgments

This research was supported by the Director, Office of Science, Office of Basic Energy Sciences, Division of Materials Science and Engineering, of the U.S. Department of Energy under Contract No. DE-AC03-76SF00098.

The authors acknowledge the support of the staff, especially Dr. Tamara Radetic, and facilities at the National Center for Electron Microscopy, along with the assistance of Dr. Seth Taylor.

References

1. Elssner G, Korn D, and Rühle M. The influence of interface impurities on fracture energy of UHV diffusion bonded metal-ceramic bicrystals. Scr. Metall. Mater. 1994; 31 (8): 1037-42.
2. Florjancic M, Mader W, Rühle M, and Turwitt M. HREM and diffraction studies of an Al_2O_3/Nb interface. J. Phys. (Paris) 1985; 46 (C4): 129-33.
3. De Graef M, Dalgleish BJ, Turner MR, and Evans AG. Interfaces between alumina and platinum: structure, bonding and fracture resistance. Acta Metall. Mater. 1992; 40 (Suppl. issue): S333-44.
4. Korn D, Elssner G, Fischmeister HF, and Rühle M. Influence of interface impurities on the fracture energy of UHV bonded niobium-sapphire bicrystals. Acta Metall. Mater. 1992; 40 (Suppl. issue): S355-60.
5. Korn D, Elssner G, Cannon RM, and Ruhle M. Fracture properties of interfacially doped Nb-Al_2O_3 bicrystals: I, fracture characteristics. Acta Materialia 2002; 50 (15): 3881-3901.
6. Cannon RM, Korn D, Elssner G, and Ruhle M. Fracture properties of interfacially doped Nb-Al_2O_3 bicrystals: II, relation of interfacial bonding, chemistry and local plasticity. Acta Materialia 2002; 50 (15): 3903-3925.
7. Jokl ML, Vitek V, and McMahon CJ, Jr. A microscopic theory of brittle fracture in deformable solids: a relation between ideal work to fracture and plastic work. Acta Metall. 1980; 28 (11): 1479-88.
8. Cannon RM, Jayaram V, Dalgleish BJ, and Fisher RM. Microstructural and chemical components of ceramic-metal interfacial fracture energies. Electronic Packaging Materials Science II Symposium. Mater Res Soc. Palo Alto, CA, April 15-18; 1986.
9. Shalz ML, Dalgleish BJ, Tomsia AP, Cannon RM, and Glaeser AM. Ceramic joining III bonding of alumina via Cu/Nb/Cu interlayers. J. Mater. Sci. 1994; 29 (14): 3678-90.
10. Knauss D and Mader W. Chemical composition and lattice relaxations at diffusion-bonded Nb/Al_2O_3 interfaces. Ultramicroscopy 1991; 37 (1-4): 247-262.
11. Nicholas MG, Forgan RRG, and Poole DM. The adhesion of metal/alumina interfaces. J. Mater. Sci. 1968; 3: 9-14.
12. Burger K, Mader W, and Rühle M. Structure, chemistry and diffusion bonding of metal/ceramic interfaces. Ultramicroscopy 1987; 22 (1-4): 1-13.
13. Mader W and Rühle M. Electron microscopy studies of defects at diffusion-bonded Nb/Al_2O_3 interfaces. Acta Metall. 1989; 37 (3): 853-66.
14. Mayer J, Dura J, Flynn CP, and Rühle M. Electron microscopy studies of Nb-Al_2O_3 interfaces formed by molecular beam epitaxy. Surface and Coatings Technol. 1990; 43/44 (1): 199-212.
15. O'Dowd NP, Stout MG, and Shih CF. Fracture toughness of alumina-niobium interfaces: experiments and analyses. Philos. Mag. A (Phys. Cond. Matter, Defects and Mech. Prop.) 1992; 66 (6): 1037-64.
16. Rühle M. Structure and composition of metal/ceramic interfaces. J. Eur. Ceram. Soc. 1995; 16 (3): 353-65.
17. Marks RA, Chapman DR, Danielson DT, and Glaeser AM. Joining of alumina via copper/niobium/copper interlayers. Acta Mater. 2000; 48 (18-19): 4425-38.
18. Kruzic JJ, Marks RA, Yoshiya M, Glaeser AM, Cannon RM, and Ritchie RO. Fracture and fatigue behavior at ambient and elevated temperatures of alumina bonded with copper/niobium/copper interlayers. J. Am. Ceram. Soc. 2002; 85 (10): 2531-41.

19. Marks RA, Sugar JD, and Glaeser AM. Ceramic joining IV. effects of processing conditions on the properties of alumina joined via Cu/Nb/Cu interlayers. J. Mater. Sci. 2001; 36 (23): 5609-24.
20. Sugar JD, McKeown JT, Marks RA, and Glaeser AM. Liquid-film assisted formation of alumina-niobium interfaces. J. Am. Ceram. Soc. 2002; 85 (10): 2523-30.
21. Seidel J, Claussen N, and Rödel J. Reliability of alumina ceramics: effect of grain size. J. Eur. Ceram. Soc. 1995; 15 (5): 395-404.
22. Rühle M and Evans AG. Structure and chemistry of metal/ceramic interfaces. Mater. Sci. Engin. 1989; A107: 187-87.
23. Dauskardt RH, Lane M, Ma Q, and Krishna N. Adhesion and debonding of multi-layer thin film structures. Eng. Fract. Mech. 1998; 61 (1): 141-62.
24. McKeown JT, Sugar JD, Gronsky R, and Glaeser AM. Processing of alumina-niobium interfaces via liquid-film-assisted joining. Weld. J. 2005; 84 (3).
25. Massalski TB and Okamoto H, editors. Binary Alloy Phase Diagrams, 2nd ed. Materials Park, OH: ASM International; 1990.
26. Zankl R and Malter R. Phase-Equilibria In The System Copper-Niobium-Silicon. Z. Metallk. 1981; 72 (10): 720-724.
27. McKeown JT, Processing and Characterization of Alumina/Niobium Interfaces Produced via Liquid Film Assisted Joining, Department of Materials Science and Engineering, University of California, Berkeley, (2003).
28. Shaw L, Miracle D, and Abbaschian R. Microstructure and mechanical properties of metal/oxide and metal/silicide interfaces. Acta Metall. Mater. 1995; 43 (12): 4267-79.
29. Nekkanti RK and Dimiduk DM. Ductile-phase toughening in niobium–niobium silicide powder processed composites. In: Anton DL, Martin PL, Miracle DB, and McMeeking R, editors. Materials Research Society Symposium Proceedings, vol. 194, Intermetallic Matrix Composites. Pittsburgh, PA: Materials Research Society; 1990, p. 175-82.

Figure Captions

Figure 1: Optical micrograph of a sapphire-niobium interface in cross-section. Copper particles persist at the interface after the bonding cycle, shown at a larger scale in the inset.

Figure 2: SEM image of a sapphire-niobium interface in cross-section.

Figure 3: Optical micrograph of a high-purity alumina–niobium interface in cross-section. The interface is free of secondary phases.

Figure 4: SEM image of a high-purity alumina-niobium interface in cross-section. Note the rough interface, due to penetration of the niobium into the alumina grain-boundary grooves and other surface irregularities.

Figure 5: Optical micrograph of a lower-purity alumina-niobium interface in cross-section. Silicide precipitates are evident at the interface. The boxes labeled "a" and "b" are the regions shown in the SEM images of Figures 6 and 7, respectively.

Figure 6: SEM image of niobium silicide precipitates at the alumina-niobium interface and slightly away from the interface at alumina grain boundaries.

Figure 7: SEM image of a niobium silicide precipitate at the alumina-niobium interface and extending away from the interface along an alumina grain boundary.

Figure 8: Bright-field TEM image of a niobium silicide precipitate extending from the alumina-niobium interface into the alumina along a grain boundary.

Figure 9: Bright-field TEM image of a niobium silicide precipitate away from the alumina-niobium interface at an alumina grain boundary.

Figure 10: EDS spectrum obtained in the SEM from the region indicated. The precipitate is a niobium silicide.

Figure 11: EDS spectra obtained in the TEM from the regions indicated. The composition of the precipitate in the grain at the alumina-niobium interface (*top spectrum*) is consistent with the Nb_5Si_3 phase. The Nb:Si ratio is lower away from the interface (*bottom spectrum*).

Figures

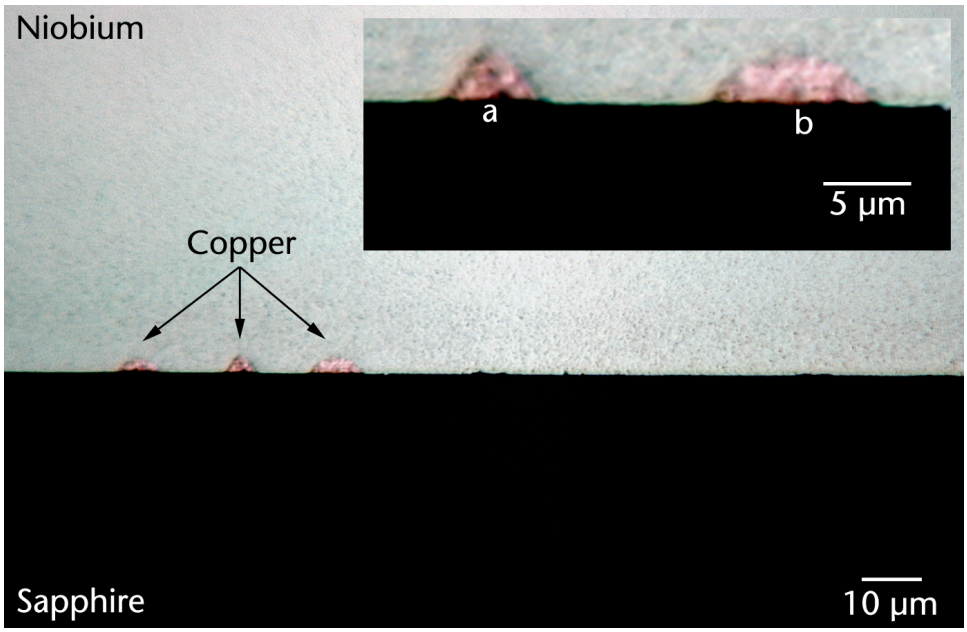

Figure 1: Optical micrograph of a sapphire-niobium interface in cross-section. Copper particles persist at the interface after the bonding cycle, shown at a larger scale in the inset.

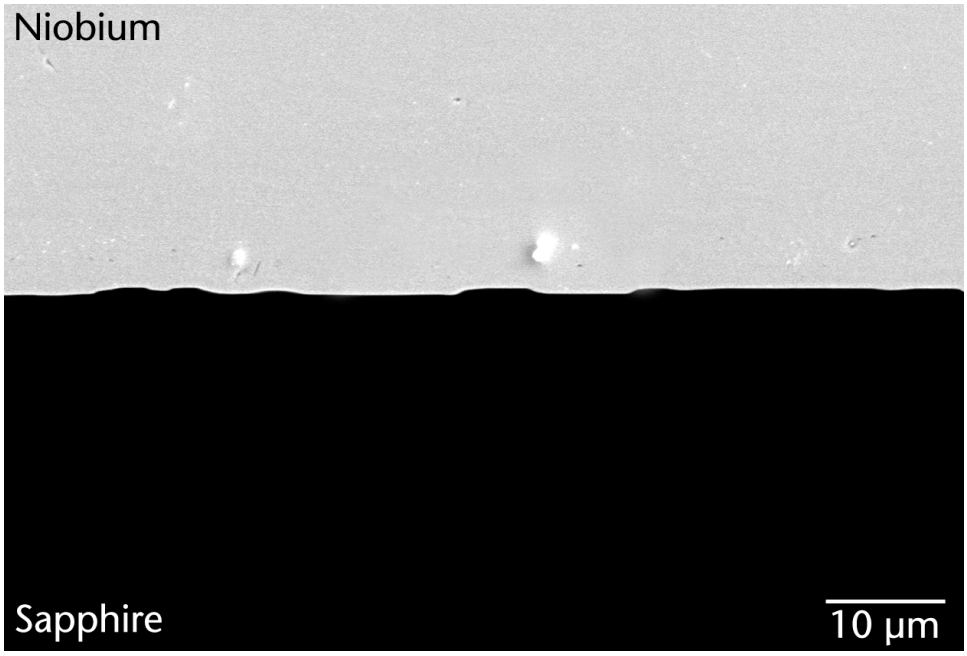

Figure 2: SEM image of a sapphire-niobium interface in cross-section.

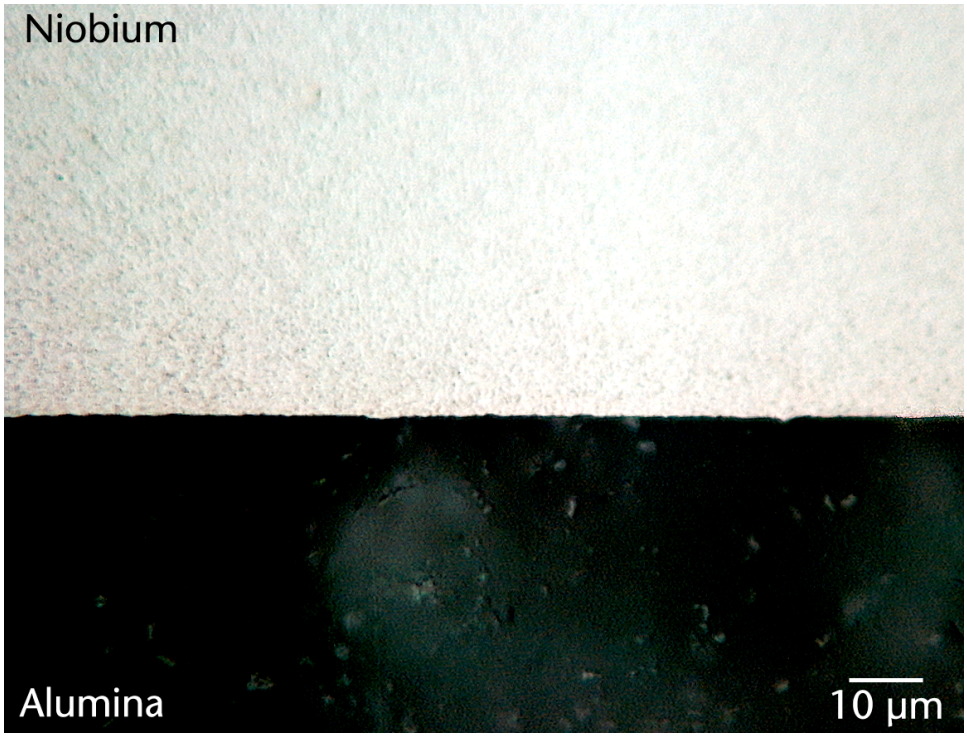

Figure 3: Optical micrograph of a high-purity alumina–niobium interface in cross-section. The interface is free of secondary phases.

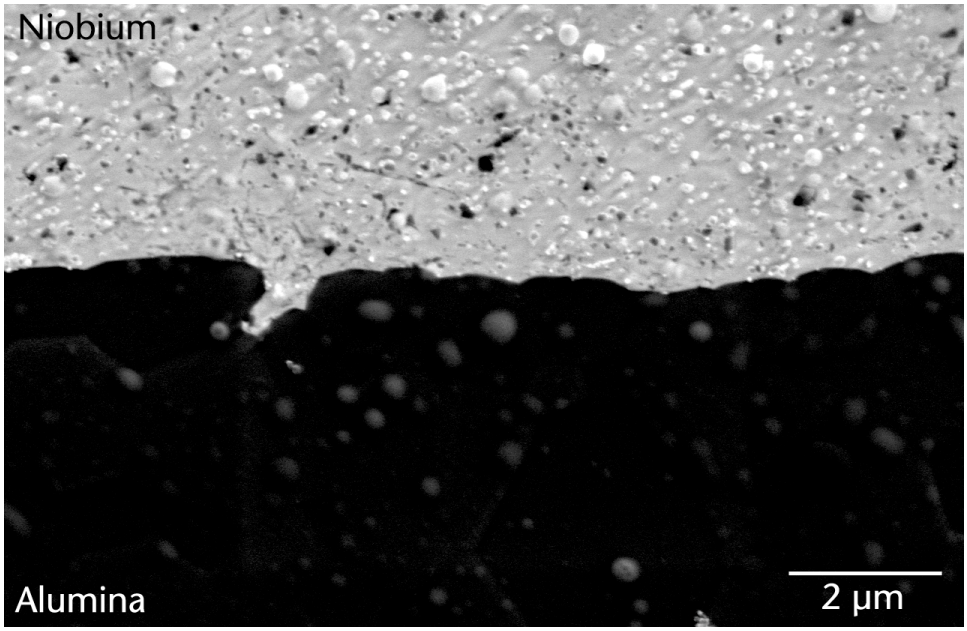

Figure 4: SEM image of a high-purity alumina-niobium interface in cross-section. Note the rough interface, due to penetration of the niobium into the alumina grain-boundary grooves and other surface irregularities.

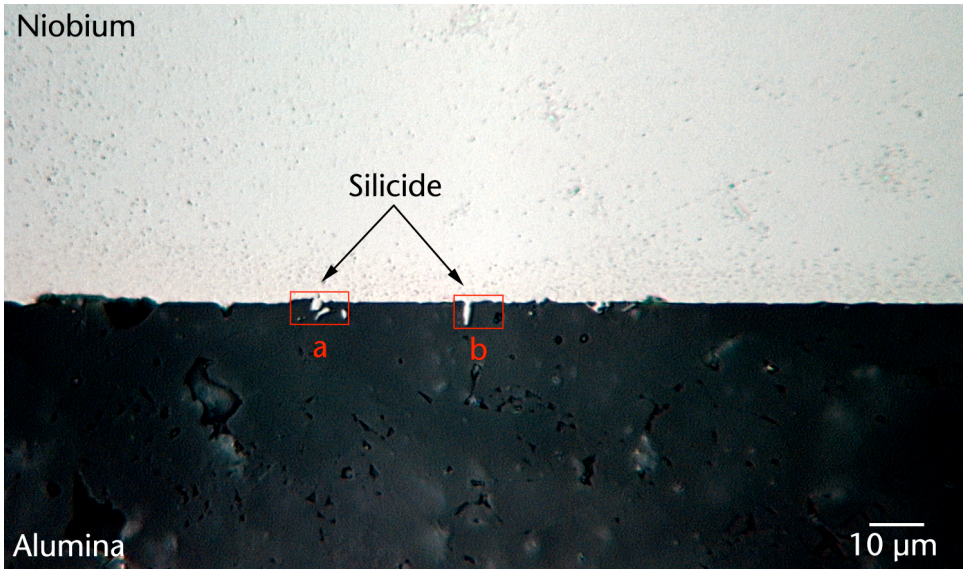

Figure 5: Optical micrograph of a lower-purity alumina-niobium interface in cross-section. Silicide precipitates are evident at the interface. The boxes labeled "a" and "b" are the regions shown in the SEM images of Figures 6 and 7, respectively.

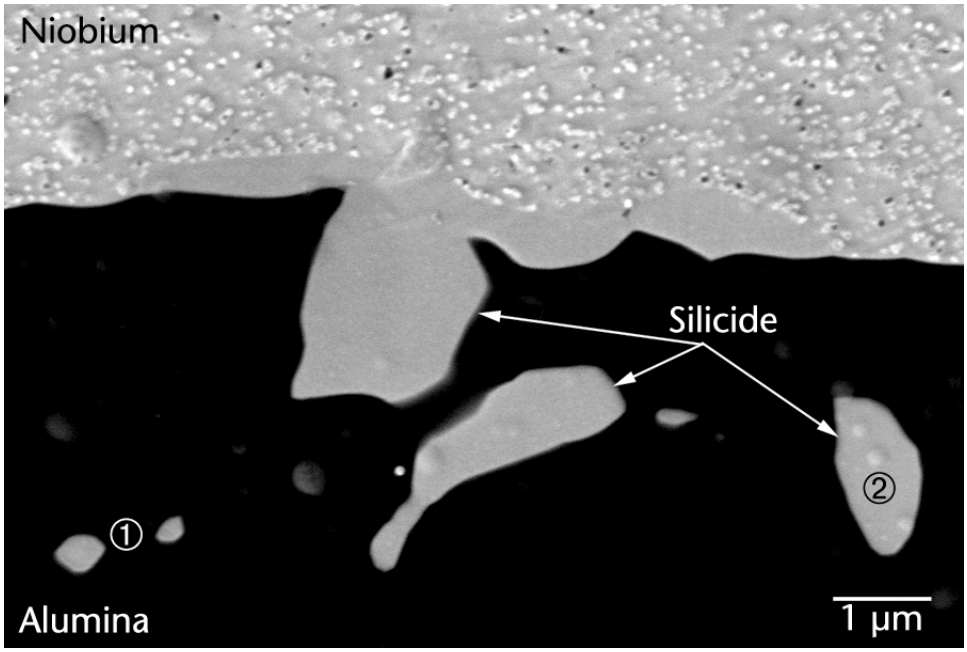

Figure 6: SEM image of niobium silicide precipitates at the alumina-niobium interface and slightly away from the interface at alumina grain boundaries.

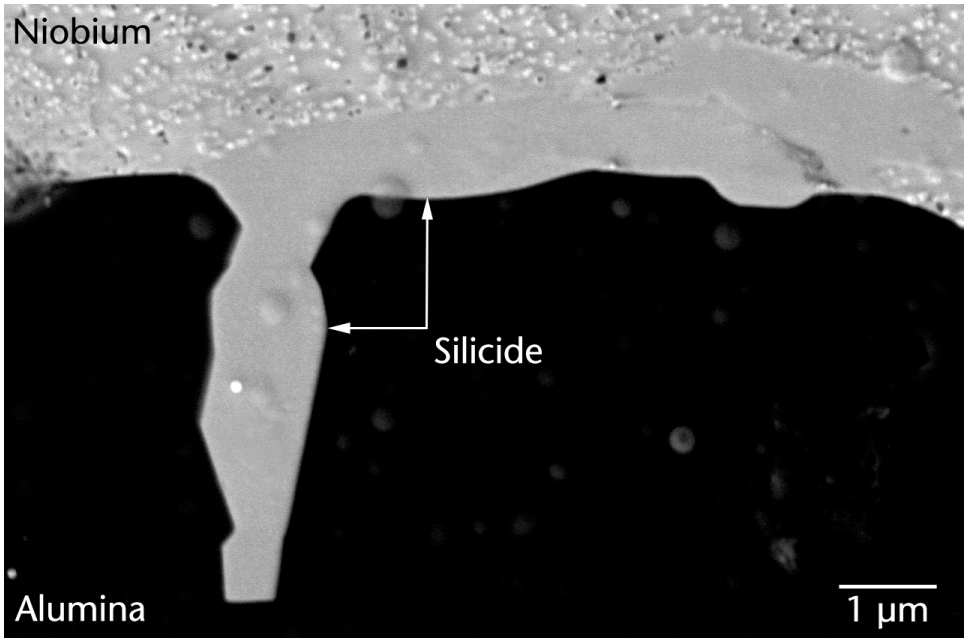

Figure 7: SEM image of a niobium silicide precipitate at the alumina-niobium interface and extending away from the interface along an alumina grain boundary.

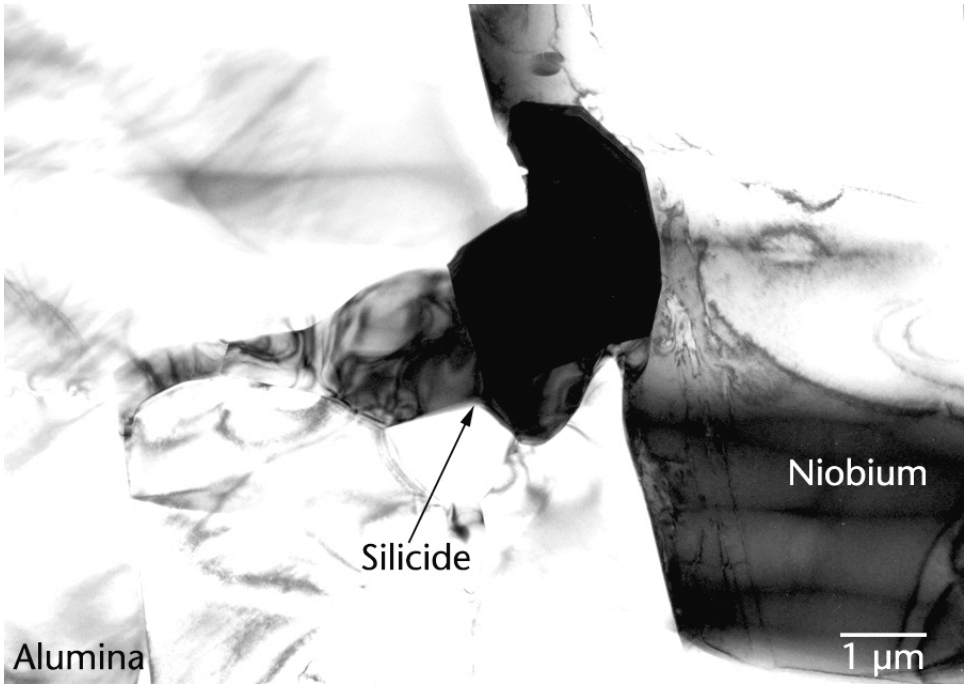

Figure 8: Bright-field TEM image of a niobium silicide precipitate extending from the alumina-niobium interface into the alumina along a grain boundary.

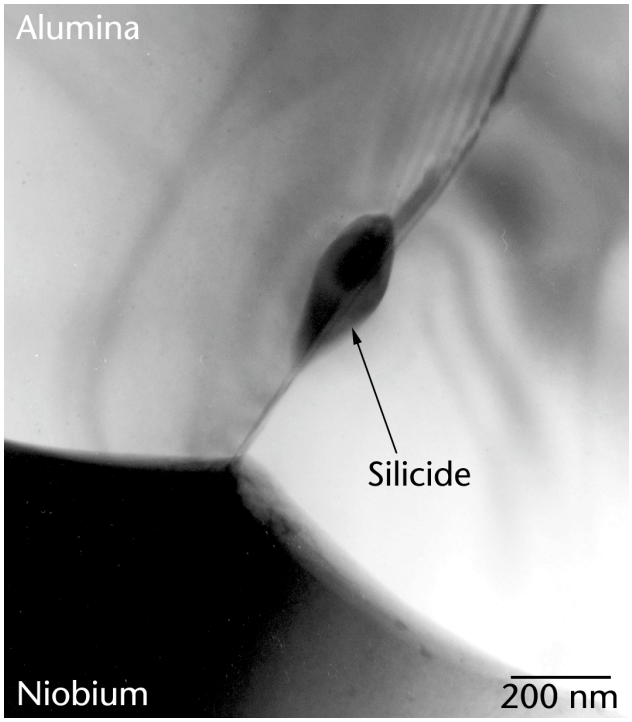

Figure 9: Bright-field TEM image of a niobium silicide precipitate away from the alumina-niobium interface at an alumina grain boundary.

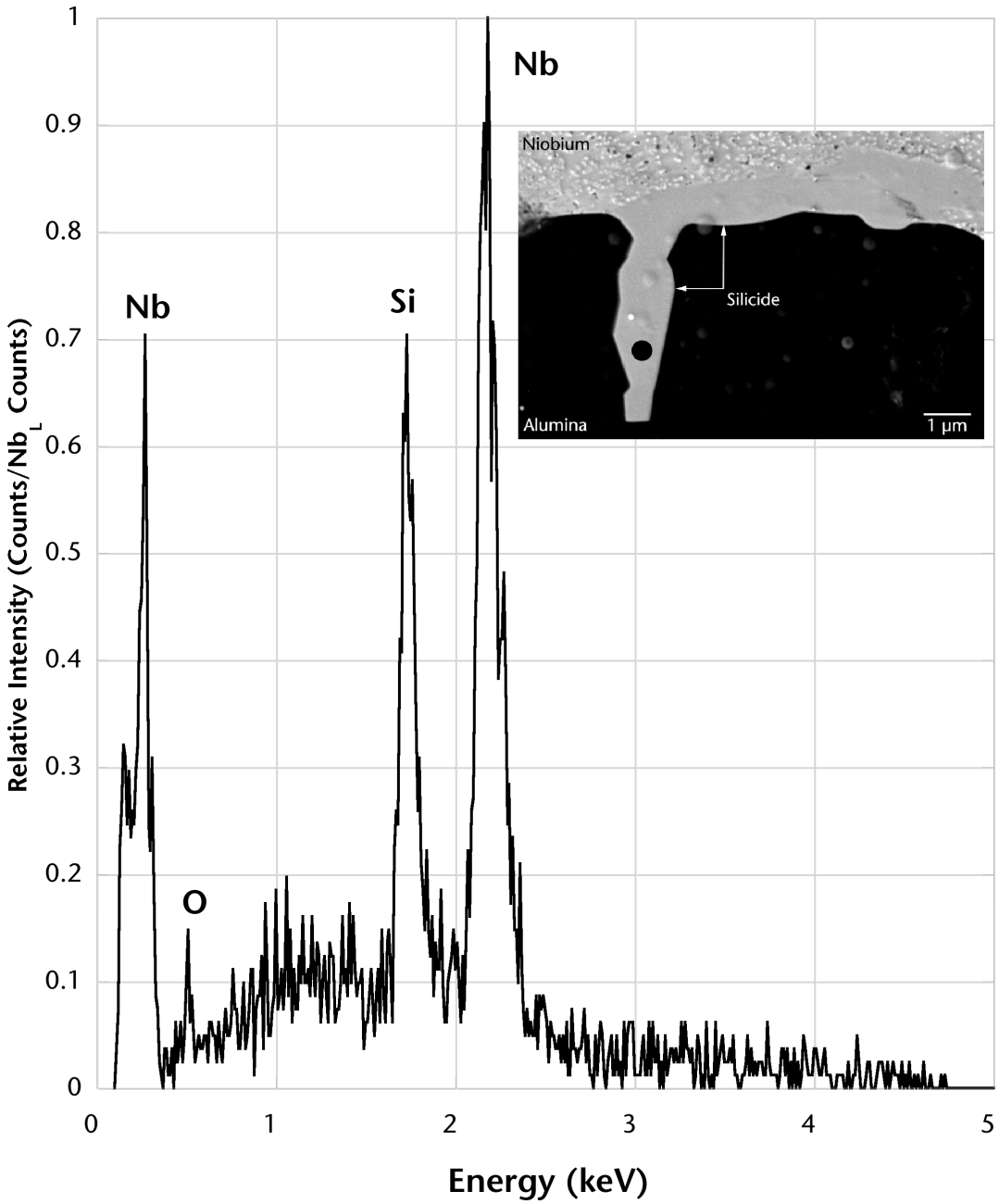

Figure 10: EDS spectrum obtained in the SEM from the region indicated. The precipitate is a niobium silicide.

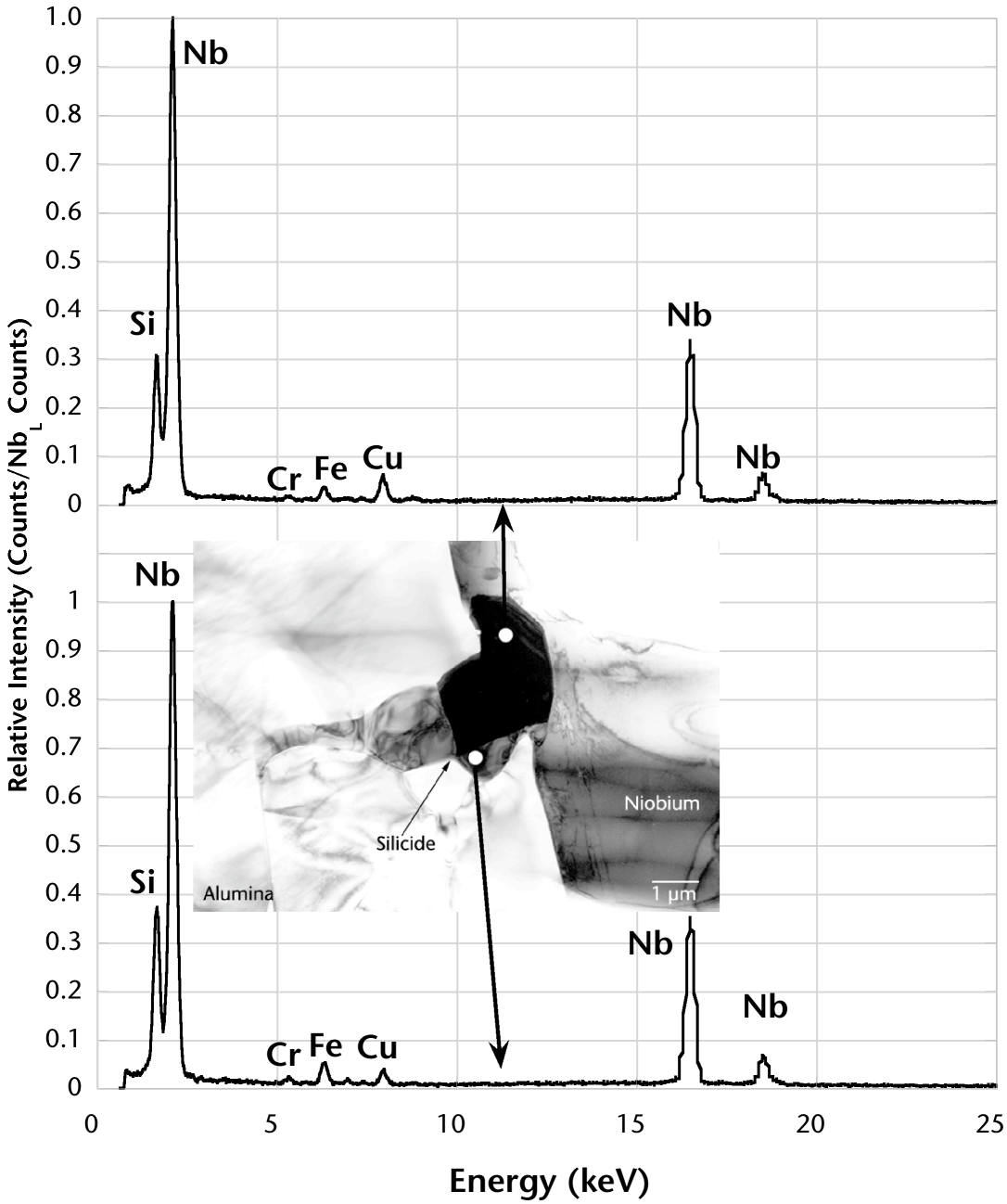

Figure 11: EDS spectra obtained in the TEM from the regions indicated. The composition of the precipitate in the grain at the alumina-niobium interface (*top spectrum*) is consistent with the Nb_5Si_3 phase. The Nb:Si ratio is lower away from the interface (*bottom spectrum*).